Environmental Science & Technology

Article

Cite This: Environ. Sci. Technol. 2019, 53, 13748−13756

pubs.acs.org/est

Significant Seasonal Variations in Isotopic Composition of Atmospheric Total Gaseous Mercury at Forest Sites in China Caused by Vegetation and Mercury Sources

Xuewu Fu,*[,†,‡] Hui Zhang,[†,§] Chen Liu,[†,§] Hui Zhang,[†] Che-Jen Lin,[∥] and Xinbin Feng*[,†,‡,§]

[†]State Key Laboratory of Environmental Geochemistry, Institute of Geochemistry, Chinese Academy of Sciences, Guiyang 550081, China

[‡]CAS Center for Excellence in Quaternary Science and Global Change, Xi'an, Shaanxi 710061, China

[§]University of Chinese Academy of Sciences, Beijing 100049, China

[∥]Center for Advances in Water and Air Quality, Lamar University, Beaumont, Texas 77710-0024, United States

Supporting Information

ABSTRACT: In this study, isotopic compositions of atmospheric total gaseous mercury (TGM) were measured in the Mt. Changbai (MCB) temperate deciduous forest and the Mt. Ailao (MAL) subtropical evergreen forest over a 1-year period. Higher $\delta^{202}Hg_{TGM}$ values were observed under the forest canopy than above the forest canopy in the MCB forest. The vertical gradients in $\delta^{202}Hg_{TGM}$ and $\Delta^{199}Hg_{TGM}$ are positively correlated with the satellite-based normalized difference vegetation index (NDVI, representing the vegetation photosynthetic activity), suggesting that a strong vegetation activity (high NDVI) induces both mass-dependent and mass-independent fractionation of TGM isotopes. The observed $\delta^{202}Hg_{TGM}$ and $\Delta^{199}Hg_{TGM}$ showed seasonal variations. Mean $\delta^{202}Hg_{TGM}$ and $\Delta^{199}Hg_{TGM}$ in summer were 0.35−0.99‰ and 0.06−0.09‰ higher than those in other seasons in the MCB forest. In contrast, the highest seasonal $\delta^{202}Hg_{TGM}$ in the MAL forest was observed in winter at 0.07−0.40‰ higher than the values found in other seasons. The variability of $\delta^{202}Hg_{TGM}$ and $\Delta^{199}Hg_{TGM}$ in MCB was attributed to vegetation activities, whereas the seasonal $\delta^{202}Hg_{TGM}$ in the MAL forest was driven by the exposure of air masses to anthropogenic emissions. Using the data in this study and in the literature, we concluded that vegetation activity and anthropogenic Hg release are the main drivers for the spatial variations in TGM isotopic compositions in the northern hemisphere.

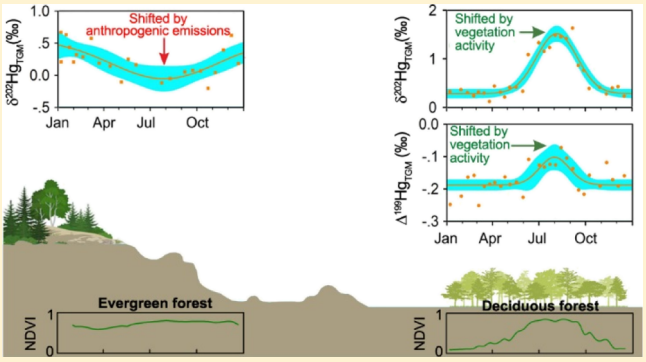

1. INTRODUCTION

Mercury (Hg) is a highly toxic heavy metal pollutant and can be transported globally in the atmosphere.[1] Hg in the atmosphere mainly exists in three operationally defined forms: gaseous elemental mercury (GEM), gaseous oxidized mercury (GOM), and particulate bound mercury (PBM). The sum of GEM and GOM is known as total gaseous mercury (TGM). GEM is the dominant form of Hg in the atmosphere, which is moderately stable and can spread globally through atmospheric circulation.[2] In addition to wet and dry deposition of GOM and PBM, dry deposition of GEM is also an important source of Hg to ecosystems and poses a concern for bioaccumulation once it transforms and enters the food web.[3−5]

Hg exists in the environment in seven stable isotopes (Hg^{196}, Hg^{198}, Hg^{199}, Hg^{200}, Hg^{201}, Hg^{202}, Hg^{204}). Laboratory and field studies have revealed that environmental processes can induce mass-dependent Hg isotope fractionation (MDF) and mass-independent fractionation (MIF) of odd-mass-number and even-mass-number Hg isotopes.[6−20] Hg is therefore a three-dimensional isotopic tracer that provides valuable clues for tracing the Hg biogeochemical cycle of Hg and its environmental and geological processes.

Concentration of TGM can be affected by anthropogenic and natural emissions as well as atmospheric transformations. Anthropogenic sources emit GEM with negative $\delta^{202}Hg$ signatures (−1.79 to −0.44‰) and near-zero $\Delta^{199}Hg$ signatures (−0.06 to 0.02‰).[21−23] The isotopic signatures of GEM emitted from natural sources, including soil and water emissions, biomass burning, and volcanic emission,[24] although not well constrained, have been predicted to have negative $\delta^{202}Hg$ values (mean = −0.40 to −2.84‰).[6,22,25,26] Atmospheric processes such as foliar uptake, oxidation, and reduction in the gaseous and particulate phase could also shift the isotopic compositions of TGM.[17,18,27,28] Therefore, both

Received: August 20, 2019
Revised: October 25, 2019
Accepted: November 4, 2019
Published: November 4, 2019

DOI: 10.1021/acs.est.9b05016
Environ. Sci. Technol. 2019, 53, 13748−13756

emission sources and atmospheric processes can contribute to the variation of the isotopic compositions of TGM. Recent studies in urban areas of the northern hemisphere found that the isotopic compositions of TGM/GEM were characterized by negative δ^{202}Hg values (mean = −0.72 to −0.08‰) and close to zero Δ^{199}Hg values (mean = −0.03 to 0.04‰),[17,29] similar to those estimated for anthropogenic GEM emissions and implicating anthropogenic emissions as the main GEM pollution sources.[21] In contrast, the isotopic signatures of GEM in remote areas were mostly characterized by slightly negative to highly positive δ^{202}Hg values (mean = −0.21 to 1.20‰) and negative Δ^{199}Hg values (mean = −0.24 to −0.12‰),[17,18,22,27,29,30] suggesting influences from atmospheric processes. However, relationships between the observed isotopic signatures and emissions/transformations have not been established, making it difficult to understand the contributing factors shifting the isotopic compositions of TGM/GEM.

In this study, TGM concentration and its isotopic signatures were measured in a temperate deciduous forest and a subtropical evergreen forest in China for over a 1-year period. The relationships between TGM isotopic compositions and anthropogenic sources, vegetation activity, biomass burning, and oceanic sources are investigated. The objectives of this study are to investigate the drivers responsible for the seasonal patterns of TGM isotopic compositions and to examine the factors contributing to the isotopic shifts of atmospheric Hg. The data obtained in this study were combined with those reported in the literature to identify the major factors influencing the spatial variation of TGM isotopic compositions in the northern hemisphere. The findings in this study help understand the controls on the variations in TGM concentrations and isotopic compositions at local, regional, and hemispheric scales.

2. METHODS

2.1. Sites' Description. The Mt. Changbai (MCB) forest [128.113° E, 42.400° N, 741 m above sea level (a.s.l.)] is a temperate deciduous broadleaved/conifer mixed forest in Northeastern China near the border with North Korea. The Mt. Ailao (MAL) forest (101.020° E, 24.533° N, 2450 m a.s.l.) is a subtropical evergreen broadleaved forest in Southwestern China near the borders of Myanmar, Laos, and Vietnam (Figure S1). Detailed information regarding the climate, potential sources, and forest structure and composition of the two forests have been reported elsewhere.[31−33] Briefly, the MCB forest is a piedmont plain forest in the middle latitude with strong seasonal variability in vegetation activity, whereas the MAL forest is a montane forest in the low latitude with relatively small seasonal variability in vegetation activity (Figure S1). To investigate the effect of vegetation activity on the fractionation of Hg isotopes in the atmosphere, two sampling sites, one under the forest canopy and the other above, were selected in the MCB forest. The sampling site in the MAL forest was located under forest canopy (1 m a.g.l.). There are no point sources within 20 km around the sampling sites or in surrounding areas.

2.2. Sampling, Preconcentration, and Determination of TGM. TGM was collected using chlorine-impregnated activated carbon (CLC, 0.5 g) traps at a flow rate of 2.0−2.5 L min^{-1}.[34] Sampling of TGM was conducted from April 2015 to April 2016 in the MCB forest and from January 2017 to February 2018 in the MAL forest with a sampling duration of approximately 2 weeks (Table S1). TGM under and above the forest canopy in the MCB forest was collected by mounting the Teflon tubing inlets at heights of 1 m and 25 m a.g.l., respectively. TGM under the forest canopy in the MAL forest was collected by mounting the Teflon tubing inlet at a height of 1 m a.g.l. The sampling inlets were connected to CLC traps, vacuum pumps, and air flow control systems in sequence using 1/4 in. Teflon tubes,[29] which were housed in temperature-controlled field laboratories in the forests. During sampling, Teflon filters (47 mm diameter; 0.2 μm pore size) were placed at the sampling inlet to remove atmospheric particulates. Immediately after the field sampling, CLC traps were sealed with silicone stoppers and three successive polyethylene bags and kept in screw-capped glass bottles in the field labs.

TGM collected on CLC traps was preconcentrated into 5 mL of 40% mixed acid solution (v/v, $2HNO_3$/1HCl) using a double-stage combustion method developed before for Hg isotope analysis.[34,35] After the preconcentration, all trapping bottles and impingers were rinsed three times with a total volume of 5 mL of Milli-Q water. The rinsed Milli-Q waters were then added to the trapping solutions. The final trapping solutions were kept in a refrigerator at 2−4 °C until Hg isotope analysis.

Hg concentrations in trapping solutions were analyzed using a cold vapor atomic fluorescence spectroscopy method. TGM concentrations of each sample were calculated by dividing the total Hg mass collected (ng) by the cumulative sampling air volume (m^3 under standard temperature of 273.14 K and pressure of 1013 hPa). Full procedural blanks of the sampling and preconcentration were determined to be 0.024 ± 0.006 ng mL^{-1} (1σ, n = 10) by combusting 0.5 g of clean CLC traps, which were negligible (<2%) compared to the Hg concentrations in field sample trapping solutions. Combustion of lichen CRM (BCR 482) using the double-stage combustion method showed a mean recovery of 94.2 ± 4.1% (1σ, n = 6). The full recoveries of TGM collection and preconcentration were tested by laboratory extractions of Hg from diluted NIST SRM 3133 solutions (volume = 2.5 L, Hg concentration: 2−20 ng L^{-1}, n = 10) onto CLC traps using Hg-free air at a purging flow rate of 2.5 L min^{-1} within 1 h, followed by preconcentration of Hg on CLC traps to trap solutions using the double-stage combustion method.[34] Mean recovery of the laboratory addition and preconcentration was 92.3 ± 4.6% (1σ, n = 10). During the sampling of the TGM isotope, atmospheric TGM concentrations were continuously measured using the automated Tekran 2537 Hg vapor analyzers at open sties adjacent to the TGM isotope sampling sites in MCB and MAL, respectively.[31,32] The mean TGM concentrations in MCB (1.57 ± 0.42, 1σ) and MAL (1.64 ± 0.81, 1σ) forests measured by the Tekran 2537 analyzers were similar to those measured by CLC traps in MCB (above canopy: mean = 1.48 ± 0.19, 1σ) and MAL (under canopy: mean = 1.70 ± 0.41, 1σ), respectively. This indicates that the CLC trap can effectively capture TGM in the atmosphere over the sampling durations (~2 weeks) without inducing significant bias in TGM isotopic compositions.[34]

2.3. Mercury Isotope Analysis. Isotope ratios of TGM in trap solutions were analyzed by cold vapor-multicollector inductively coupled plasma mass spectrometry (CV-MC-ICPMS, Nu Instruments, U.K.) at the State key Laboratory of Environmental Geochemistry, CAS (Guiyang, China). Before Hg isotope analysis, the final trap solution was diluted to a concentration containing approximately 1 ng mL^{-1} Hg,

DOI: 10.1021/acs.est.9b05016
Environ. Sci. Technol. 2019, 53, 13748−13756

which matched within 10% of the bracketing standard NIST SRM 3133 concentration (1.0 ng mL^{-1}). The diluted trap solutions and 3% $SnCl_2$ were introduced inline to a cold vapor phase separator (Figure S2), and then the reduced Hg^0 together with a Tl aerosol (used for instrumental mass bias correction) generated by a desolvating nebulizer (Aridus II, Cetac) were carried by Argon carrier gas to MC-ICPMS. The signal intensity of Hg detected by MC-ICPMS during the whole analytical sessions ranged from 1.10 to 1.32 V per ng mL^{-1} of Hg. Isotopic ratios were corrected for mass bias by standard−sample−standard bracketing using the international standard NIST SRM 3133. Isotopic compositions of TGM are expressed in delta notation (δ) in per mil (‰) referenced to the bracketing standard NIST SRM 3133[36]

$$\delta^{xxx}\mathrm{Hg}_{\mathrm{TGM}}\ (‰) = \left[\frac{\left(\frac{^{xxx}\mathrm{Hg}}{^{198}\mathrm{Hg}}\right)_{\mathrm{sample}}}{\left(\frac{^{xxx}\mathrm{Hg}}{^{198}\mathrm{Hg}}\right)_{\mathrm{NIST\ SRM\ 3133}}} - 1\right] \times 1000 \quad (1)$$

where *xxx* refers to the mass of each Hg isotope between 199 and 202 (Hg^{204} was not measured because of the limitations of instrumental collector designs). MIF values are expressed in capital delta notation (Δ), which are the deviations of the measured isotopic compositions from those theoretically predicted from δ^{202}Hg using the kinetic MDF law[36]

$$\Delta^{xxx}\mathrm{Hg}_{\mathrm{TGM}}\ (‰) = \delta^{xxx}\mathrm{Hg}_{\mathrm{sample}} - \beta \times \delta^{202}\mathrm{Hg}_{\mathrm{sample}} \quad (2)$$

where *xxx* are the mass of Hg isotope ^{199}Hg, ^{200}Hg, and ^{201}Hg, and β values are 0.252, 0.502, and 0.752 for isotopes ^{199}Hg, ^{200}Hg, and ^{201}Hg, respectively.

The analytical uncertainty of the TGM isotopic analysis was assessed by repeated analysis of the isotopic compositions of NIST SRM 3177 (n = 22), lichen CRM (BCR 482, n = 6), and standard addition of NIST SRM 3133 to CLC traps (n = 10) over different analytical sessions. Overall, the measured isotopic compositions of NIST SRM 3177, lichen CRM, and standard addition of NIST SRM 3133 to CLC traps were consistent with previously reported values (Table S2).[37,38] Analytical uncertainty on TGM isotopic compositions was influenced by field collection, laboratory preconcentration, and instrumental procedures. The laboratory control experiments with NIST SRM 3133 Hg isotope addition to CLC traps represented the analytical uncertainty associated with TGM isotopic compositions measurements. Therefore, the analytical uncertainty (2σ) of TGM isotopic compositions reported in this study is the larger 2σ value of either the standard addition of NIST SRM 3133 to CLC traps or repeated analysis of the TGM sample over different analytical sessions.

2.4. Quantification of Vegetation Activity, Anthropogenic Hg Emission, Biomass Burning, and Oceanic Air Mass. To investigate the factors that control the variations in TGM isotopic compositions, we analyzed the local normalized difference vegetation index (NDVI), cumulative NDVI ($\sum$NDVI), cumulative anthropogenic Hg^0 emission ($\sum Hg^0$ emission), cumulative wildfire ($\sum$fire), and fractional air mass residence time (ARTs) over the ocean for each TGM isotope sample in MCB and MAL (Supporting Information, Text S1). The local NDVI, representing the vegetation activity in the surrounding areas of MCB and MAL,[39] was obtained from the global gridded NDVI data (from the National Aeronautic and Space Administration Earth Observation platform at 16 days temporal and 0.1° spatial resolution) at 0.5° × 0.5° resolution at the sampling sites. The analysis of $\sum$NDVI, $\sum Hg^0$ emission, $\sum$fire, and fractional oceanic ARTs was utilized to determine the magnitude of TGM isotopic compositions influenced by air masses passing over vegetation, anthropogenic Hg^0 sources, active fires, and oceans, respectively. The origins and atmospheric transport of air masses of each TGM isotope sample were calculated using the TrajStat Geographical Information System-based software and gridded meteorological data (Global Data Assimilation System, GDAS1) from the U.S. National Oceanic and Atmospheric Administration (NOAA),[40] which are further used to determine the prior exposure of air to vegetation activity (represented by NDVI), anthropogenic Hg^0 emissions,[41] active fires (data from the National Aeronautic and Space Administration Earth Observation platform at 8 days temporal and 0.1° spatial resolution), and oceans. Meteorological parameters including wind speed, relative humidity, air temperature, and solar radiation in MCB and MAL forests were obtained from the meteorological stations in the Open Research Station of the Changbai Mountain Forest Ecosystem and Ailao Mountain Forest Ecosystem, both located within 500 m of the sampling sites.

The mean $\sum$NDVI (trajectory-based) were positively correlated with the local mean NDVI in MCB (r^2 = 0.93, p < 0.01) and MAL (r^2 = 0.95, p < 0.01) forests (Figure S3). In the MCB forest, the mean $\sum$NDVI in May and June 2015 were lower (0.04−0.31) than the local NDVI, possibly because the air masses were mainly originated from high latitudes, where vegetation activity was still low during late spring and early summer. Mean $\sum$NDVI, mean $\sum Hg^0$ emission, mean $\sum$fire and fractional oceanic ARTs based on the 48 h backward trajectory were all consistent with that based on the 24 and 120 h backward trajectory (Figures S4 and S5), suggesting that the use of 48 h backward trajectory at the sampling sites is appropriate to investigate the effects of vegetation activity and Hg sources on isotopic compositions of TGM.

3. RESULTS AND DISCUSSION

3.1. TGM Concentrations in MCB and MAL Forests. Mean ($\pm 1\sigma$) TGM concentrations measured using activated carbon traps under (1 m a.s.l.) and above (25 m a.s.l.) the forest canopy in the MCB forest from April 2015 to April 2016 were 1.44 ± 0.23 ng m^{-3} (n = 29) and 1.48 ± 0.19 ng m^{-3} (n = 29), respectively (Table S3). The mean ($\pm 1\sigma$) TGM concentration under the forest canopy (1 m a.s.l.) in the MAL forest from January 2017 to February 2018 was 1.70 ± 0.41 ng m^{-3} (n = 22) (Table S3). TGM concentrations in MCB and MAL forests were close to the mean background value of 1.55 ng m^{-3} in 2013 in the northern hemisphere,[42] but slightly higher than the mean ($\pm 1\sigma$) of 1.40 ± 0.14 ng m^{-3} (1 σ, n = 18) observed at the forest sites in North America and Europe.[5,18,39,43,44] Significant seasonal variations of TGM concentrations were observed in both MCB and MAL forests (K-independent sample t-test, p < 0.01 or <0.05, Table S3). The seasonal variation in TGM concentrations is most likely controlled by Hg emissions, atmospheric transformations, and transport and vegetation activities.[39,45−48] In MCB, mean TGM concentrations under the forest canopy were the lowest in summer (1.25 ± 0.18 ng m^{-3}) because of the higher vegetative uptake of GEM in the leaf-growing season and the lower exposure of air to anthropogenic sources (Table S3).[39,49]

DOI: 10.1021/acs.est.9b05016
Environ. Sci. Technol. 2019, 53, 13748−13756

In contrast, the mean TGM concentration in MAL was the lowest in winter (1.48 ± 0.40 ng m^{-3}), possibly associated with the lesser influence of air masses containing anthropogenic emissions from southwestern China (Table S3).[32,49,50]

3.2. TGM Isotopic Compositions. TGM samples in MCB and MAL forests were generally characterized by positive δ^{202}Hg values and negative Δ^{199}Hg and Δ^{200}Hg values (Figure 1 and Table S1). For example, δ^{202}Hg of TGM varied from

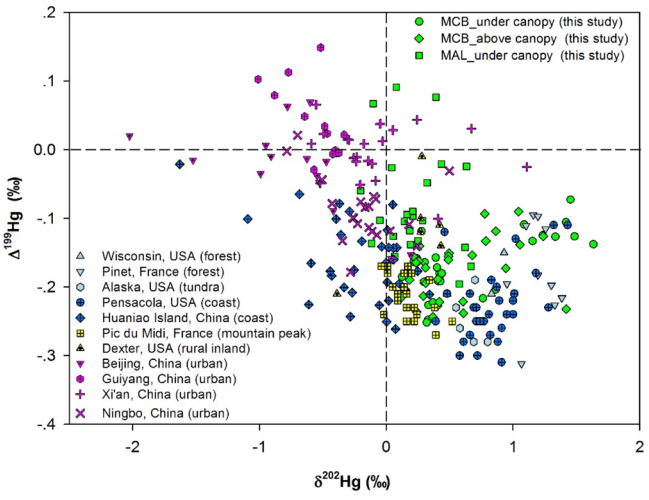

Figure 1. Mass-dependent (δ^{202}Hg) and mass-independent (Δ^{199}Hg) isotope signatures of atmospheric TGM/GEM worldwide. Data are from this study and the literatures.[4,5,17,18,22,23,27,29,30]

0.12 to 1.64‰ (mean [±1σ] = 0.66 ± 0.47‰, n = 29) under the canopy and from 0.12 to 1.42‰ (mean [±1σ] = 0.52 ± 0.35‰, n = 29) above the canopy in MCB, and from −0.20 to 0.67‰ (mean [±1σ] = 0.17 ± 0.25‰, n = 22) under the canopy in MAL (Figure 1). The Δ^{199}Hg of TGM varied from −0.24 to −0.09‰ (mean [±1σ] = −0.17 ± 0.04‰, n = 29) under the canopy and from −0.24 to −0.09‰ (mean [±1σ] = −0.18 ± 0.04‰, n = 29) above the canopy in MCB, and from −0.20 to 0.09‰ (mean [±1σ] = −0.08 ± 0.08‰, n = 22) under the canopy in MAL (Figure 1). Mean Δ^{200}Hg of TGM at the three sites ranged from −0.07 to −0.03‰ (Table S3).

The annual means of $\delta^{202}Hg_{TGM}$ in MCB and MAL were lower than the values previously observed at forest sites in summer, and the annual means of $\Delta^{199}Hg_{TGM}$ in MCB and MAL were similar to or higher than those observed at forest sites in summer (e.g., Wisconsin, United States and Pinet, France, mean $\delta^{202}Hg_{TGM}$ and $\Delta^{199}Hg_{TGM}$ varied from 0.75 to 1.19‰ and −0.19 to −0.17‰, respectively, Figure 1).[5,18] Global observations at forest sites showed the mean $\delta^{202}Hg_{TGM}$ and $\Delta^{199}Hg_{TGM}$ values of 0.67 ± 0.35‰ (1σ, n = 5) and −0.16 ± 0.04‰ (1σ, n = 5), respectively. The mean of $\delta^{202}Hg_{TGM}$ at global forest sites was higher than those observed at rural sites not surrounded by forests (e.g., coastal and high-altitude sites, mean $\delta^{202}Hg_{TGM}$ = 0.22 ± 0.47‰ (1σ, n = 6), Figure 1) and urban sites (mean $\delta^{202}Hg_{TGM}$ = −0.39 ± 0.30‰ (1σ, n = 4), Figure 1).[4,17,22,23,27,29,30] This implies that environmental processes within the forests shifted the isotopic composition of TGM toward higher δ^{202}Hg values, which is further discussed in the following sections. The mean $\Delta^{199}Hg_{TGM}$ at global forest sites was similar to those found at rural sites not surrounded by forests [mean = −0.18 ± 0.06‰ (1σ, n = 6)],[17,22,27,29,30] but lower than those at global urban sites [mean = −0.02 ± 0.05‰ (1σ, n = 4)].[23,29] The means of $\Delta^{200}Hg_{TGM}$ at remote sites worldwide varied slightly from −0.10 to −0.03‰ (n = 10) and were lower than those observed at urban sites (means = −0.01 to 0.01‰, n = 4).[4,5,17,18,22,23,27,29,30]

3.3. Vertical Gradient in $\delta^{202}Hg_{TGM}$ and $\Delta^{199}Hg_{TGM}$ in the MCB Forest. Vertical gradients in TGM concentrations and isotopic compositions were measured under and above the canopy in the MCB forest. The gradients in TGM concentrations (Δ-TGM = TGM_{1m} − TGM_{25m}) ranged from −0.20 to 0.11 ng m^{-3} during the 1-year period (mean [±1σ] = −0.04 ± 0.09 ng m^{-3}, n = 27, Figure 2). Depositions of TGM

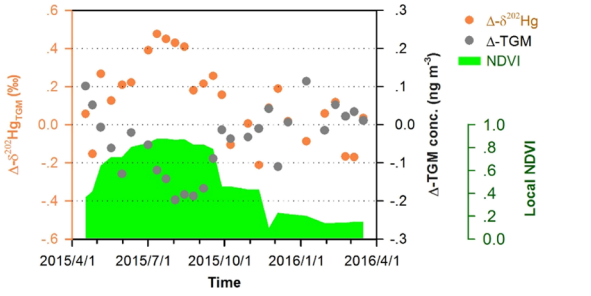

Figure 2. Temporal variations in vertical gradient in atmospheric TGM δ^{202}Hg values (Δ-$\delta^{202}Hg_{TGM}$ = $\delta^{202}Hg_{TGM\text{-}1m}$ − $\delta^{202}Hg_{TGM\text{-}25m}$), vertical gradient in atmospheric TGM concentrations (Δ-TGM = TGM_{1m} − TGM_{25m}), and mean local vegetation activity (NDVI) in the MCB forest.

onto vegetation, characterized by negative Δ-TGM values, were mostly observed after early spring at the start of the leaf-growing season and lasted until the end of autumn. Emissions of TGM in the forest (positive Δ-TGM values) were mainly observed in winter and early spring, possibly associated with re-emission of the deposited Hg.[4,51] Seasonal variation in TGM gradients was significant (K-independent sample t-test, p < 0.01). The lowest seasonal mean of Δ-TGM concentrations (−0.13 ± 0.07 ng m^{-3}, 1σ) appeared in summer, corresponding to a net TGM deposition of ∼9% in the forest. Means of Δ-TGM concentrations in spring, autumn, and winter were 0.00 ± 0.08, −0.04 ± 0.07, and 0.01 ± 0.07 ng m^{-3}, respectively. The Δ-TGM concentrations were negatively correlated with local NDVI analysis of variance (ANOVA, r^2 = 0.58, p < 0.01, Figure 3A) and relative humidity (ANOVA, r^2 = 0.32, p < 0.01), and significantly positively correlated with wind speed (ANOVA, r^2 = 0.25, p < 0.01). The dry deposition of TGM onto vegetation in MCB exhibited a maximum in summer when the vegetation activity and air relative humidity were highest and the wind speed was lowest (Table S3). This is possibly caused by the enhanced foliar uptake of Hg^0 in the presence of high vegetation activity and high relative humidity and the shallow boundary layers caused by low wind speeds.[33,52] High air temperature and solar radiation in summer can enhance the emission/re-emission of TGM from foliage and forest soil,[19,53] and therefore are not expected to contribute to the higher deposition of TGM in summer. A forward stepwise multiple regression analysis between Δ-TGM concentrations and environmental variables mentioned above showed that NDVI and relative humidity most significantly influenced the seasonal variation in TGM gradients (ANOVA, p < 0.05 for both), which explained 58 and 9% of the variation in TGM gradients, respectively (a total of 67%). These two variables are tightly linked to the vegetation uptake of TGM,

DOI: 10.1021/acs.est.9b05016
Environ. Sci. Technol. 2019, 53, 13748−13756

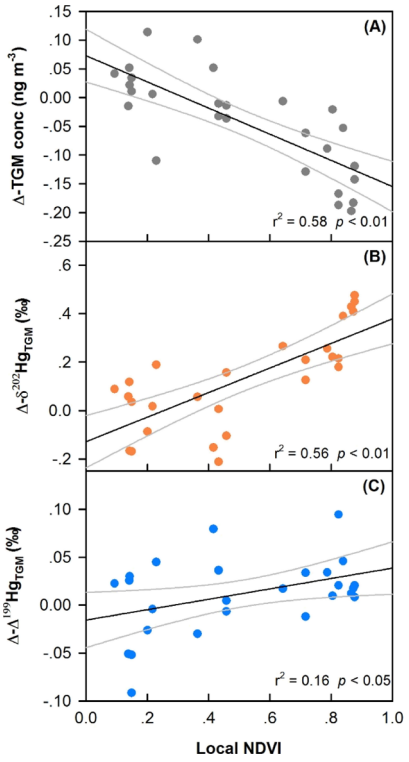

Figure 3. Effect of vegetation activities on the gradient in TGM concentrations and isotopic compositions in the MCB forest. (A) Δ-TGM concentration vs NDVI, (B) Δ-$\delta^{202}Hg_{TGM}$ vs NDVI, and (C) Δ-$\Delta^{199}Hg_{TGM}$ vs NDVI. Black lines represent the linear regression of the data and the gray lines are the 95% confidence line of the regression.

suggesting that vegetation activities dominated the deposition of TGM in the forest.

The mean ($\pm 1\sigma$) gradients in TGM isotopic compositions (n = 27) in MCB were 0.13 ± 0.20‰ for Δ-$\delta^{202}Hg_{TGM}$ ($\delta^{202}Hg_{TGM\text{-}1m} - \delta^{202}Hg_{TGM\text{-}25m}$), 0.01 ± 0.04‰ for Δ−$\Delta^{199}Hg_{TGM}$ ($\Delta^{199}Hg_{TGM\text{-}1m} - \Delta^{199}Hg_{TGM\text{-}25m}$), and 0.02 ± 0.04‰ for Δ-$\Delta^{200}Hg_{TGM}$ ($\Delta^{200}Hg_{TGM\text{-}1m} - \Delta^{200}Hg_{TGM\text{-}25m}$) (Figures 2 and S6). A significant seasonal variation in Δ-$\delta^{202}Hg_{TGM}$ was observed (K-independent sample t-test, p < 0.01) with the summertime mean (0.37 ± 0.12‰, 1σ) much higher than other seasons (means = 0.02 to 0.06‰, n = 3). The Δ-$\delta^{202}Hg_{TGM}$ values in the MCB forest were positively correlated with the local NDVI (Figure 3B), which explains 56% of Δ-$\delta^{202}Hg_{TGM}$ variations and indicates the strong vegetation activity contributing to a positive shift of $\delta^{202}Hg_{TGM}$ values under the forest canopy in MCB. A forward stepwise multiple regression analysis between the Δ-$\delta^{202}Hg_{TGM}$ and environmental variables including local NDVI and meteorological parameters did show insignificant statistical relationships between Δ-$\delta^{202}Hg_{TGM}$ and meteorological parameters (ANOVA, p values for all >0.05), indicating that meteorological parameters were not the primary drivers for the temporal variations in Δ-$\delta^{202}Hg_{TGM}$. A Rayleigh fractionation model using an MDF fractionation factor of −2.89‰ between TGM and the foliage reported by Demers et al.[18] can fit the observed relationship between Δ-$\delta^{202}Hg_{TGM}$ values and TGM_{1m}/TGM_{25m} ratios (net fraction of TGM remaining after passing through the forest canopy) (ANOVA, r^2 = 0.42, p < 0.01, Figure S7). A deposition of 9% of TGM because of foliage uptake would predict a mean $\delta^{202}Hg_{TGM}$ increase of ~0.29‰ under the forest canopy in summer, close to the observed mean Δ-$\delta^{202}Hg_{TGM}$ value in summer (0.37 ± 0.12‰, 1σ). It has been reported that MDF can occur during the air−foliage exchange of TGM. The data shown in this study provide direct evidence that this process could notably modify the MDF signatures of TGM within the forest ambient air when there is a high vegetation activity.

Seasonal variations in Δ-$\Delta^{199}Hg_{TGM}$ and Δ-$\Delta^{200}Hg_{TGM}$ were insignificant (K-independent sample t-test, p(Δ-$\Delta^{199}Hg_{TGM}$) = 0.43, p(Δ-$\Delta^{200}Hg_{TGM}$) = 0.97, Figure S6). The seasonal means of Δ-$\Delta^{199}Hg_{TGM}$ and Δ-$\Delta^{200}Hg_{TGM}$ ranged from −0.01 to 0.03‰ (n = 4) and 0.02−0.03‰ (n = 4), respectively. A weak but significant positive correlation was observed between Δ-$\Delta^{199}Hg_{TGM}$ and local NDVI (Figure 3C). The slight increase of Δ-$\Delta^{199}Hg_{TGM}$ during the leaf-growing season was likely caused by the re-emission of Hg previously incorporated into foliage (most likely characterized by moderate positive Δ^{199}Hg values).[18,19]

Exchange of Hg^0 between forest soil and the atmosphere may also have contributed to the vertical gradients in TGM isotopic compositions. Soil−air exchange of Hg^0 exhibited strong seasonality with higher emission in summer because of relative higher temperature and solar radiation.[54,55] Isotopic fractionation during air−soil exchange of Hg^0 had not been extensively studied. Previous studies suggested that adsorption and oxidation of Hg^0 by soil organic matter can result in a strong positive δ^{202}Hg and a small positive Δ^{199}Hg in the atmospheric TGM pool.[18,56] In contrast, photochemical and biological reduction of Hg in forest soil had been shown to release Hg^0 with negative δ^{202}Hg and a complicated Δ^{199}Hg signature (negative or positive depending on Hg complex in forest soil),[57] offsetting the MDF and MIF fractionation patterns during adsorption and oxidation of Hg^0 by soil organic matter. In MCB, forest soil is as a net source (mean = 2.8 ng m^{-2} h^{-1}) of TGM in summer,[33] which was likely induced by reduction and evaporation processes and therefore would possibly result in a negative shift of δ^{202}Hg in TGM.[7,57] This is not the case found in this study, suggesting that the exchange of Hg^0 between forest soil and the atmosphere was not the main cause for the positive shift of $\delta^{202}Hg_{TGM}$ under the forest canopy. On the other hand, a positive shift in Δ^{199}Hg values under the forest canopy may be related to photoreduction of Hg from sulfur-containing ligands within leaf litter,[15] but fractionation during foliage/air exchange cannot be ruled out. Further field observations on MDF and MIF fractionation of Hg^0 during air−soil exchange are needed to evaluate the contribution of soil evasion to the isotopic signatures of TGM.

3.4. Causes of Seasonal Variations in TGM Isotopic Compositions. The values of $\delta^{202}Hg_{TGM}$ and $\Delta^{199}Hg_{TGM}$ in MCB and $\delta^{202}Hg_{TGM}$ in MAL showed significant seasonal variations (K-independent sample t-test, p < 0.01 or <0.05, Figure 4 and 5). Seasonal variations of $\Delta^{199}Hg_{TGM}$ in MAL and $\Delta^{200}Hg_{TGM}$ in MCB and MAL were not statistically significant (K-independent sample t-test, p > 0.05 for all, Figures 5 and S8). In MCB, the seasonal variations of $\delta^{202}Hg_{TGM}$ and $\Delta^{199}Hg_{TGM}$ were similar in both sampling locations (below and above the canopy, Figures 4 and 5). The highest mean $\delta^{202}Hg_{TGM}$ above (0.92 ± 0.18‰, 1σ) and under canopy (1.31 ± 0.15‰, 1σ) were observed in summer. This was 0.35−0.65‰ and 0.63−0.99‰ higher than the means in other seasons, respectively (Table S3). The highest mean $\Delta^{199}Hg_{TGM}$ above (−0.13 ± 0.03‰, 1σ) and under the canopy (−0.11 ± 0.02‰, 1σ) was also observed in summer, 0.06−0.07‰ and

DOI: 10.1021/acs.est.9b05016
Environ. Sci. Technol. 2019, 53, 13748−13756

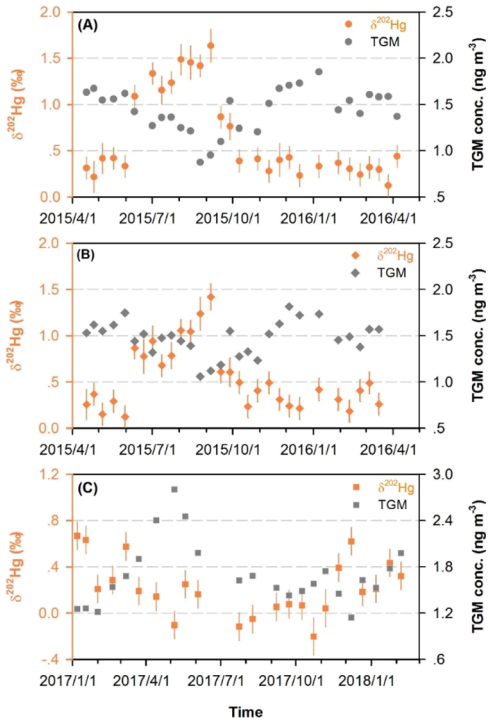

Figure 4. Seasonal variations in atmospheric TGM δ^{202}Hg and TGM concentrations at sites of (A) under the forest canopy (1 m a.s.l) in MCB, (B) above the forest canopy (25 m a.s.l) in MCB, and (C) under the forest canopy in MAL.

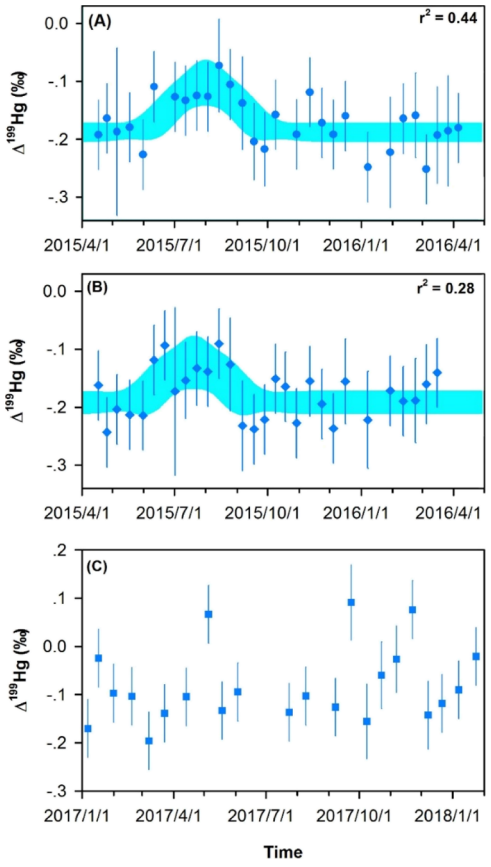

Figure 5. Seasonal variations in atmospheric TGM Δ^{199}Hg at sites of (A) under the forest canopy (1 m a.s.l) in MCB, (B) above the forest canopy (25 m a.s.l) in MCB, and (C) under the forest canopy in MAL. The shaded area is the 95% confidence area of the Gaussian regression of data.

0.06−0.09‰ higher than those in other seasons, respectively (Table S3). In contrast, $\delta^{202}Hg_{TGM}$ at MAL showed the lowest mean (0 ± 0.15‰, 1σ) in summer, which was 0.07−0.40‰ lower than the values in other seasons (Table S3).

In MCB, $\delta^{202}Hg_{TGM}$ were highly correlated with ∑NDVI, which explained 61 and 76% of the seasonal variability above and under the forest canopy, respectively (ANOVA, $p < 0.01$ for both, Figure S9). A weak but significant negative correlation existed between $\delta^{202}Hg_{TGM}$ and mean $\sum Hg^0$ emission (ANOVA, $r^2 = 0.20$, $p < 0.05$ for both, Figure S9), suggesting that exposure of air masses to anthropogenic emission sources can shift the isotopic composition of TGM toward lower δ^{202}Hg values as observed elsewhere.[22,27,30] There were no significant correlations between $\delta^{202}Hg_{TGM}$ above and under the forest canopy in MCB and mean ∑fire (ANOVA, $p > 0.05$ for both, Figure S9) or oceanic ARTs (ANOVA, $r^2 = 0.10$, $p = 0.10$, Figure S9). A forward stepwise multiple regression analysis between $\delta^{202}Hg_{TGM}$ and ∑NDVI, $\sum Hg^0$ emission, ∑fire, and fractional oceanic ARTs showed that the mean ∑NDVI was the only dominant factor controlling the seasonal variations of $\delta^{202}Hg_{TGM}$ above and under the forest canopy in MCB (ANOVA, $p < 0.01$), whereas the roles of other factors are insignificant (ANOVA, $p > 0.05$ for all). In MAL, $\delta^{202}Hg_{TGM}$ under the forest canopy were inversely correlated with mean $\sum Hg^0$ emission (ANOVA, $r^2 = 0.35$, $p < 0.01$, Figure S9), whereas other factors (∑NDVI, ∑fire, and fractional oceanic ARTs) were insignificant (ANOVA, $p > 0.05$ for all, Figure S9). This suggests that anthropogenic emission ($\sum Hg^0$ emission) was the main controlling factor of the seasonal variations of $\delta^{202}Hg_{TGM}$ in MAL, in contrast to the vegetation activity in MCB.

$\Delta^{199}Hg_{TGM}$ above and under the forest canopy in MCB were both weakly correlated with mean ∑NDVI (ANOVA, $p < 0.05$ or <0.01, Figure S10). This is consistent with the observed vertical gradient in $\Delta^{199}Hg_{TGM}$ caused by vegetation activity that leads to a positive shift of Δ^{199}Hg in TGM. The correlation was stronger under the canopy ($r^2 = 0.39$, $p < 0.01$, Figure S10) than that above the canopy ($r^2 = 0.15$, $p < 0.05$, Figure S10). The $\Delta^{199}Hg_{TGM}$ above and under the forest canopy in MCB were also correlated with fractional oceanic ARTs (ANOVA, $p < 0.05$ for both, Figure S10). Oceanic ARTs in MCB during the study period mostly originated from Bohai Sea and Yellow Sea (Figure S11). These regions were frequently impacted by the outflow of primary anthropogenic emissions from mainland China and had elevated TGM concentrations (mean = 2.61 ± 0.50 ng m^{-3}, 1 sd) compared to the background level in the northern hemisphere.[58−60] Therefore, the atmospheric TGM pool in these regions is possibly characterized by lesser negative Δ^{199}Hg values compared to the global background atmospheric TGM pool and more air masses passing through these oceanic regions might shift $\Delta^{199}Hg_{TGM}$ positively in MCB.[21,22] There were insignificant correlations between $\Delta^{199}Hg_{TGM}$ in MCB and mean $\sum Hg^0$ emission or mean ∑fire (ANOVA, p values >0.05 for all, Figure S10), suggesting that anthropogenic sources and biomass burning played a minor role in the seasonal variability of $\Delta^{199}Hg_{TGM}$ in MCB. $\Delta^{199}Hg_{TGM}$ in MAL did not show significant correlation with mean ∑NDVI, mean $\sum Hg^0$ emission, mean ∑fire, and fractional oceanic ARTs (ANOVA, p values >0.05 for all, Figure S10). It is likely that

DOI: 10.1021/acs.est.9b05016
Environ. Sci. Technol. 2019, 53, 13748−13756

the control of a single source or vegetation activity was confounded by other processes at the sampling site and/or during atmospheric transport.

The stable isotope data of TGM provide observational evidence pointing to the vegetation activity as the key driver for the seasonal variations of $\delta^{202}Hg_{TGM}$ and $\Delta^{199}Hg_{TGM}$ in the temperate deciduous forest in Northeast China, shifting the isotopic composition of TGM toward higher $\delta^{202}Hg_{TGM}$ and $\Delta^{199}Hg_{TGM}$ values. In contrast, transport of anthropogenic emissions was identified as the key driver for the seasonal variations of $\delta^{202}Hg_{TGM}$ in the subtropical evergreen forest in the Southwest China. Note that this finding does not imply that vegetation activity is unimportant in influencing the isotopic composition of TGM in the subtropical evergreen forest. The lack of significant correlation between $\delta^{202}Hg_{TGM}$ and the vegetation activity in MAL was partially owing to its small seasonal amplitude in $\sum$NDVI (($\sum NDVI_{max} - \sum NDVI_{min}$)/$\sum NDVI_{mean}$) (33%, ~5 times lower than that in MCB (171%), Figures S9 and S10). On the other hand, seasonal amplitude in $\sum Hg^0$ emission ($\sum Hg^0$ $emission_{max} - \sum Hg^0 emission_{min}$)/$\sum Hg^0 emission_{mean}$) was much higher in MAL (~210%) than that in MCB (~99%) (Figures S9 and S10). As the $\delta^{202}Hg$ signature of anthropogenic sources is generally distinctly different from those of the background TGM pool,[17,21,22] the seasonal transport of anthropogenic emissions led to the shift of $\delta^{202}Hg_{TGM}$ in MAL.

3.5. Implications for Global Distributions in the Isotopic Composition of TGM. Jiskra et al.[39] investigated the role of vegetation activity in global TGM seasonality and found that TGM concentrations co-vary with vegetation activity at background sites in the northern hemisphere. Deposition of TGM because of vegetation activity is accompanied by positive shifts of $\delta^{202}Hg_{TGM}$ and $\Delta^{199}Hg_{TGM}$ (Figure 3). Given the isotopic shifts, higher values of $\delta^{202}Hg_{TGM}$ and $\Delta^{199}Hg_{TGM}$ in summer are anticipated in widespread terrestrial regions. Year-round observations of TGM isotopic compositions remain limited in the literature. Previous studies were mostly conducted in unforested areas where peak $\delta^{202}Hg_{TGM}$ occurred in winter or spring (e.g., Pic du Midi Observatory in France and Xi'an, Guiyang, and Ningbo in China), except in Beijing (peaked in autumn) (Table S4).[23,27,29] The wintertime and springtime $\delta^{202}Hg_{TGM}$ peaks cannot be explained by the vegetation activity, which is comparatively weak in the cold seasons. At Pic du Midi, the highest wintertime mean of $\delta^{202}Hg_{TGM}$ was likely a result of little exposure of air masses to anthropogenic emissions (Table S4). At urban sites, the wintertime and springtime peaks in $\delta^{202}Hg_{TGM}$ were not associated with decreasing $\sum Hg^0$ emission (Table S4), indicating that there were other processes responsible for the observed seasonal variations in $\delta^{202}Hg_{TGM}$. $\Delta^{199}Hg_{TGM}$ at urban sites did not have strong seasonality, possibly owing to the dominant control of anthropogenic emissions throughout the year ($\sum Hg^0$ emission ranged from 123 to 511 kg/0.5 grid/h, which were much higher than remote sites, Tables S3 and S4).

Observations at global sites showed the means of $\delta^{202}Hg_{TGM}$ and $\Delta^{199}Hg_{TGM}$ ranging from −0.73 to 1.19‰ and from −0.25 to 0.06‰ (n = 15), respectively (Figure 1). We found that the means of $\delta^{202}Hg_{TGM}$ at these sites are inversely correlated with the mean $\sum Hg^0$ emission (ANOVA, r^2 = 0.51, p < 0.01) and positively correlated with NDVI (ANOVA, r^2 = 0.32, p < 0.05) (Figure S12). Cumulative anthropogenic emissions and vegetation activity combined can explain 70% of the global spatial variations found in $\delta^{202}Hg_{TGM}$ (ANOVA, p < 0.01, Figure S13). At these sites, significant correlations were found between the mean $\Delta^{199}Hg_{TGM}$ and mean $\sum Hg^0$ emission (ANOVA, r^2 = 0.40, p < 0.05) but not between mean $\Delta^{199}Hg_{TGM}$ and NDVI (ANOVA, r^2 = 0.05, p = 0.41) (Figure S12). These results confirm that anthropogenic emissions and vegetation activity are two important drivers for the temporal and spatial variations in TGM isotopic compositions, although they may not be the only plausible factors. The influence on the isotopic concentrations of TGM by natural Hg^0 emissions and atmospheric transformations are not considered in this study and cannot be ruled out. Presently, the isotopic endmembers of these sources/processes are not appropriately constrained and require further characterization in future studies. Such data will advance our understanding on the factors controlling the spatial and temporal variations of TGM isotopic compositions at regional and global scales.

■ ASSOCIATED CONTENT

Supporting Information

The Supporting Information is available free of charge on the ACS Publications website at DOI: 10.1021/acs.est.9b05016.

Additional information of the study sites, data of TGM concentrations and isotopic compositions, Rayleigh fractionation model fitting, isotopic compositions of Hg in soil and foliage, origins of air masses, analysis of the effect of anthropogenic emission and vegetation activities on the variations of TGM isotopic composition (PDF)

■ AUTHOR INFORMATION

Corresponding Authors

*E-mail: fuxuewu@mail.gyig.ac.cn. Phone: +86 851 85891508. Fax: +86 851 85891609 (Xuewu Fu).

*E-mail: fengxinbin@vip.skleg.cn. Phone: +86 851 85891356. Fax: +86 851 85891609 (Xinbin Feng).

ORCID

Xuewu Fu: 0000-0002-5174-7150

Xinbin Feng: 0000-0002-7462-8998

Notes

The authors declare no competing financial interest.

■ ACKNOWLEDGMENTS

This work was funded by the "National Key R&D Program of China (2017YFC0212001)", the Strategic Priority Research Program of Chinese Academy of Sciences, Pan-Third Pole Environment Study for a Green Silk Road (Pan-TPE, XDA20040501), the National Science Foundation of China (41622305 and 41829701), the Chinese Academy of Sciences (ZDBS-LY-DQC029, 2017443), and the K.C. Wong Education Foundation.

■ REFERENCES

(1) Obrist, D.; Kirk, J. L.; Zhang, L.; Sunderland, E. M.; Jiskra, M.; Selin, N. E. A review of global environmental mercury processes in response to human and natural perturbations: Changes of emissions, climate, and land use. *Ambio* **2018**, *47*, 116−140.

(2) Gustin, M. S.; Amos, H. M.; Huang, J.; Miller, M. B.; Heidecorn, K. Measuring and modeling mercury in the atmosphere: a critical review. *Atmos. Chem. Phys.* **2015**, *15*, 5697−5713.

(3) Zheng, W.; Gilleaudeaua, G. J.; Kah, L. C.; Anbar, A. D. Mercury isotope signatures record photic zone euxinia in the Mesoproterozoic ocean. *Proc. Natl. Acad. Sci. U.S.A.* **2018**, *115*, 10594−10599.
(4) Obrist, D.; Agnan, Y.; Jiskra, M.; Olson, C. L.; Colegrove, D. P.; Hueber, J.; Moore, C. W.; Sonke, J. E.; Helmig, D. Tundra uptake of atmospheric elemental mercury drives Arctic mercury pollution. *Nature* **2017**, *547*, 201−204.
(5) Enrico, M.; Le Roux, G.; Marusczak, N.; Heimburger, L. E.; Claustres, A.; Fu, X. W.; Sun, R. Y.; Sonke, J. E. Atmospheric Mercury Transfer to Peat Bogs Dominated by Gaseous Elemental Mercury Dry Deposition. *Environ. Sci. Technol.* **2016**, *50*, 2405−2412.
(6) Bergquist, B. A.; Blum, J. D. Mass-dependent and -independent fractionation of hg isotopes by photoreduction in aquatic systems. *Science* **2007**, *318*, 417−420.
(7) Zheng, W.; Foucher, D.; Hintelmann, H. Mercury isotope fractionation during volatilization of Hg(0) from solution into the gas phase. *J. Anal. At. Spectrom.* **2007**, *22*, 1097−1104.
(8) Kritee, K.; Blum, J. D.; Barkay, T. Mercury Stable Isotope Fractionation during Reduction of Hg(II) by Different Microbial Pathways. *Environ. Sci. Technol.* **2008**, *42*, 9171−9177.
(9) Estrade, N.; Carignan, J.; Sonke, J. E.; Donard, O. F. X. Mercury isotope fractionation during liquid-vapor evaporation experiments. *Geochim. Cosmochim. Acta* **2009**, *73*, 2693−2711.
(10) Kritee, K.; Barkay, T.; Blum, J. D. Mass dependent stable isotope fractionation of mercury during *mer* mediated microbial degradation of monomethylmercury. *Geochim. Cosmochim. Acta* **2009**, *73*, 1285−1296.
(11) Yang, L.; Sturgeon, R. Isotopic fractionation of mercury induced by reduction and ethylation. *Anal. Bioanal. Chem.* **2009**, *393*, 377−385.
(12) Zheng, W.; Hintelmann, H. Mercury isotope fractionation during photoreduction in natural water is controlled by its Hg/DOC ratio. *Geochim. Cosmochim. Acta* **2009**, *73*, 6704−6715.
(13) Sherman, L. S.; Blum, J. D.; Johnson, K. P.; Keeler, G. J.; Barres, J. A.; Douglas, T. A. Mass-independent fractionation of mercury isotopes in Arctic snow driven by sunlight. *Nat. Geosci.* **2010**, *3*, 173−177.
(14) Wiederhold, J. G.; Cramer, C. J.; Daniel, K.; Infante, I.; Bourdon, B.; Kretzschmar, R. Equilibrium Mercury Isotope Fractionation between Dissolved Hg(II) Species and Thiol-Bound Hg. *Environ. Sci. Technol.* **2010**, *44*, 4191−4197.
(15) Zheng, W.; Hintelmann, H. Isotope fractionation of mercury during its photochemical reduction by low-molecular-weight organic compounds. *J. Phys. Chem. A* **2010**, *114*, 4246−4253.
(16) Chen, J.; Hintelmann, H.; Feng, X. B.; Dimock, B. Unusual fractionation of both odd and even mercury isotopes in precipitation from Peterborough, ON, Canada. *Geochim. Cosmochim. Acta* **2012**, *90*, 33−46.
(17) Gratz, L. E.; Keeler, G. J.; Blum, J. D.; Sherman, L. S. Isotopic composition and fractionation of mercury in Great Lakes precipitation and ambient air. *Environ. Sci. Technol.* **2010**, *44*, 7764−7770.
(18) Demers, J. D.; Blum, J. D.; Zak, D. R. Mercury isotopes in a forested ecosystem: Implications for air-surface exchange dynamics and the global mercury cycle. *Global Biogeochem. Cycles* **2013**, *27*, 222−238.
(19) Yuan, W.; Sommar, J.; Lin, C.-J.; Wang, X.; Li, K.; Liu, Y.; Zhang, H.; Lu, Z.; Wu, C.; Feng, X. Stable Isotope Evidence Shows Re-emission of Elemental Mercury Vapor Occurring after Reductive Loss from Foliage. *Environ. Sci. Technol.* **2019**, *53*, 651−660.
(20) Sun, R.; Heimburger, L. E.; Sonke, J. E.; Liu, G. J.; Amouroux, D.; Berail, S. Mercury stable isotope fractionation in six utility boilers of two large coal-fired power plants. *Chem. Geol.* **2013**, *336*, 103−111.
(21) Sun, R.; Streets, D. G.; Horowitz, H. M.; Amos, H. M.; Liu, G. J.; Perrot, V.; Toutain, J. P.; Hintelmann, H.; Sunderland, E. M.; Sonke, J. E. Historical (1850−2010) mercury stable isotope inventory from anthropogenic sources to the atmosphere. *Elem. Sci. Anth.* **2016**, *4*, 000091.
(22) Fu, X.; Yang, X.; Tan, Q.; Ming, L.; Lin, T.; Lin, C.-J.; Li, X.; Feng, X. Isotopic Composition of Gaseous Elemental Mercury in the Marine Boundary Layer of East China Sea. *J. Geophys. Res.: Atmos.* **2018**, *123*, 7656−7669.
(23) Xu, H.; Sonke, J. E.; Guinot, B.; Fu, X.; Sun, R.; Lanzanova, A.; Candaudap, F.; Shen, Z.; Cao, J. Seasonal and Annual Variations in Atmospheric Hg and Pb Isotopes in Xi'an, China. *Environ Sci Technol* **2017**, *51*, 3759−3766.
(24) Pirrone, N.; Cinnirella, S.; Feng, X.; Finkelman, R. B.; Friedli, H. R.; Leaner, J.; Mason, R.; Mukherjee, A. B.; Stracher, G. B.; Streets, D. G.; Telmer, K. Global mercury emissions to the atmosphere from anthropogenic and natural sources. *Atmos. Chem. Phys.* **2010**, *10*, 5951−5964.
(25) Sun, R.; Jiskra, M.; Amos, H. M.; Zhang, Y. X.; Sunderland, E. M.; Sonke, J. E. Modelling the mercury stable isotope distribution of Earth surface reservoirs: Implications for global Hg cycling. *Geochim. Cosmochim. Acta* **2019**, *246*, 156−173.
(26) Zambardi, T.; Sonke, J. E.; Toutain, J. P.; Sortino, F.; Shinohara, H. Mercury emissions and stable isotopic compositions at Vulcano Island (Italy). *Earth Planet. Sci. Lett.* **2009**, *277*, 236−243.
(27) Fu, X.; Marusczak, N.; Wang, X.; Gheusi, F.; Sonke, J. E. Isotopic Composition of Gaseous Elemental Mercury in the Free Troposphere of the Pic du Midi Observatory, France. *Environ. Sci. Technol.* **2016**, *50*, 5641−5650.
(28) Fu, X.; Zhang, H.; Feng, X. B.; Tan, Q. Y.; Ming, L. L.; Liu, C.; Zhang, L. M. Domestic and Transboundary Sources of Atmospheric Particulate Bound Mercury in Remote Areas of China: Evidence from Mercury Isotopes. *Environ. Sci. Technol.* **2019**, *53*, 1947−1957.
(29) Yu, B.; Fu, X.; Yin, R.; Zhang, H.; Wang, X.; Lin, C.-J.; Wu, C.; Zhang, Y.; He, N.; Fu, P.; Wang, Z.; Shang, L.; Sommar, J.; Sonke, J. E.; Maurice, L.; Guinot, B.; Feng, X. Isotopic Composition of Atmospheric Mercury in China: New Evidence for Sources and Transformation Processes in Air and in Vegetation. *Environ. Sci. Technol.* **2016**, *50*, 9262−9269.
(30) Demers, J. D.; Sherman, L. S.; Blum, J. D.; Marsik, F. J.; Dvonch, J. T. Coupling atmospheric mercury isotope ratios and meteorology to identify sources of mercury impacting a coastal urban-industrial region near Pensacola, Florida, USA. *Global Biogeochem. Cycles* **2015**, *29*, 1689−1705.
(31) Fu, X. W.; Feng, X.; Shang, L. H.; Wang, S. F.; Zhang, H. Two years of measurements of atmospheric total gaseous mercury (TGM) at a remote site in Mt. Changbai area, Northeastern China. *Atmos. Chem. Phys.* **2012**, *12*, 4215−4226.
(32) Zhang, H.; Fu, X.; Lin, C. J.; Shang, L.; Zhang, Y.; Feng, X.; Lin, C. Monsoon-facilitated characteristics and transport of atmospheric mercury at a high-altitude background site in southwestern China. *Atmos. Chem. Phys.* **2016**, *16*, 13131−13148.
(33) Fu, X.; Zhu, W.; Zhang, H.; Sommar, J.; Yu, B.; Yang, X.; Wang, X.; Lin, C. J.; Feng, X. Depletion of atmospheric gaseous elemental mercury by plant uptake at Mt. Changbai, Northeast China. *Atmos. Chem. Phys.* **2016**, *16*, 12861−12873.
(34) Fu, X.; Heimburger, L. E.; Sonke, J. E. Collection of atmospheric gaseous mercury for stable isotope analysis using iodine- and chlorine-impregnated activated carbon traps. *J. Anal. At. Spectrom.* **2014**, *29*, 841−852.
(35) Biswas, A.; Blum, J. D.; Bergquist, B. A.; Keeler, G. J.; Xie, Z. Q. Natural mercury isotope variation in coal deposits and organic soils. *Environ. Sci. Technol.* **2008**, *42*, 8303−8309.
(36) Blum, J. D.; Bergquist, B. A. Reporting of variations in the natural isotopic composition of mercury. *Anal. Bioanal. Chem.* **2007**, *388*, 353−359.
(37) Sun, G.; Sommar, J.; Feng, X.; Lin, C.-J.; Ge, M.; Wang, W.; Yin, R.; Fu, X.; Shang, L. Mass-dependent and -independent fractionation of mercury isotope during gas-phase oxidation of elemental mercury vapor by atomic Cl and Br. *Environ. Sci. Technol.* **2016**, *50*, 9232−9241.
(38) Estrade, N.; Carignan, J.; Sonke, J. E.; Donard, O. F. X. Measuring Hg Isotopes in Bio-Geo-Environmental Reference Materials. *Geostand. Geoanal. Res.* **2010**, *34*, 79−93.
(39) Jiskra, M.; Sonke, J. E.; Obrist, D.; Bieser, J.; Ebinghaus, R.; Myhre, C. L.; Pfaffhuber, K. A.; Wangberg, I.; Kyllonen, K.; Worthy,

DOI: 10.1021/acs.est.9b05016
Environ. Sci. Technol. 2019, 53, 13748−13756

D.; Martin, L. G.; Labuschagne, C.; Mkololo, T.; Ramonet, M.; Magand, O.; Dommergue, A. A vegetation control on seasonal variations in global atmospheric mercury concentrations. *Nat. Geosci.* **2018**, *11*, 244.
(40) Wang, Y. Q.; Zhang, X. Y.; Draxler, R. R. TrajStat: GIS-based software that uses various trajectory statistical analysis methods to identify potential sources from long-term air pollution measurement data. *Environ. Model. Softw* **2009**, *24*, 938−939.
(41) AMAP/UNEP. *Geospatially Distributed Mercury Emissions Dataset 2010v1*, 2013.
(42) Sprovieri, F.; Pirrone, N.; Bencardino, M.; D'Amore, F.; Carbone, F.; Cinnirella, S.; Mannarino, V.; Landis, M.; Ebinghaus, R.; Weigelt, A.; Brunke, E. G.; Labuschagne, C.; Martin, L.; Munthe, J.; Wangberg, I.; Artaxo, P.; Morais, F.; Barbosa, H. D. J.; Brito, J.; Cairns, W.; Barbante, C.; Dieguez, M. D.; Garcia, P. E.; Dommergue, A.; Angot, H.; Magand, O.; Skov, H.; Horvat, M.; Kotnik, J.; Read, K. A.; Neves, L. M.; Gawlik, B. M.; Sena, F.; Mashyanov, N.; Obolkin, V.; Wip, D.; Bin Feng, X.; Zhang, H.; Fu, X. W.; Ramachandran, R.; Cossa, D.; Knoery, J.; Marusczak, N.; Nerentorp, M.; Norstrom, C. Atmospheric mercury concentrations observed at ground-based monitoring sites globally distributed in the framework of the GMOS network. *Atmos. Chem. Phys.* **2016**, *16*, 11915−11935.
(43) Zhang, L.; Blanchard, P.; Gay, D. A.; Prestbo, E. M.; Risch, M. R.; Johnson, D.; Narayan, J.; Zsolway, R.; Holsen, T. M.; Miller, E. K.; Castro, M. S.; Graydon, J. A.; St Louis, V. L.; Dalziel, J. Estimation of speciated and total mercury dry deposition at monitoring locations in eastern and central North America. *Atmos. Chem. Phys.* **2012**, *12*, 4327−4340.
(44) Cole, A. S.; Steffen, A.; Pfaffhuber, K. A.; Berg, T.; Pilote, M.; Poissant, L.; Tordon, R.; Hung, H. Ten-year trends of atmospheric mercury in the high Arctic compared to Canadian sub-Arctic and mid-latitude sites. *Atmos. Chem. Phys.* **2013**, *13*, 1535−1545.
(45) Selin, N. E.; Jacob, D. J.; Park, R. J.; Yantosca, R. M.; Strode, S.; Jaegle, L.; Jaffe, D. Chemical cycling and deposition of atmospheric mercury: Global constraints from observations. *J. Geophys. Res.: Atmos.* **2007**, *112*, 1−14.
(46) Slemr, F.; Brunke, E. G.; Labuschagne, C.; Ebinghaus, R. Total gaseous mercury concentrations at the Cape Point GAW station and their seasonality. *Geophys. Res. Lett.* **2008**, *35*, L11807.
(47) Rothenberg, S. E.; Mckee, L.; Gilbreath, A.; Yee, D.; Connor, M.; Fu, X. Evidence for short-range transport of atmospheric mercury to a rural, inland site. *Atmos. Environ.* **2010**, *44*, 1263−1273.
(48) Fu, X.; Marusczak, N.; Heimbürger, L.-E.; Sauvage, B.; Gheusi, F.; Prestbo, E. M.; Sonke, J. E. Atmospheric mercury speciation dynamics at the high-altitude Pic du Midi Observatory, southern France. *Atmos. Chem. Phys.* **2016**, *16*, 5623−5639.
(49) Fu, X. W.; Zhang, H.; Yu, B.; Wang, X.; Lin, C.-J.; Feng, X. B. Observations of atmospheric mercury in China: a critical review. *Atmos. Chem. Phys.* **2015**, *15*, 9455−9476.
(50) Zhang, H.; Fu, X. W.; Lin, C.-J.; Wang, X.; Feng, X. B. Observation and analysis of speciated atmospheric mercury in Shangri-La, Tibetan Plateau, China. *Atmos. Chem. Phys.* **2015**, *15*, 653−665.
(51) Ferrari, C.; Gauchard, P.; Aspmo, K.; Dommergue, A.; Magand, O.; Bahlmann, E.; Nagorski, S.; Temme, C.; Ebinghaus, R.; Steffen, A.; Banic, C.; Berg, T.; Planchon, F.; Barbante, C.; Cescon, P.; Boutron, C. F. Snow-to-air exchanges of mercury in an Arctic seasonal snow pack in Ny-Alesund, Svalbard. *Atmos. Environ.* **2005**, *39*, 7633−7645.
(52) Lindberg, S. E.; Hanson, P. J.; Meyers, T. P.; Kim, K.-H. Air/surface exchange of mercury vapor over forests-the need for a reassessment of continental biogenic emissions. *Atmos. Environ.* **1998**, *32*, 895−908.
(53) Zhu, W.; Lin, C.-J.; Wang, X.; Sommar, J.; Fu, X.; Feng, X. Global observations and modeling of atmosphere-surface exchange of elemental mercury: a critical review. *Atmos. Chem. Phys.* **2016**, *16*, 4451−4480.
(54) Ma, M.; Wang, D.; Du, H.; Sun, T.; Zhao, Z.; Wang, Y.; Wei, S. Mercury dynamics and mass balance in a subtropical forest, southwestern China. *Atmos. Chem. Phys.* **2016**, *16*, 4529−4537.
(55) Choi, H.-D.; Holsen, T. M. Gaseous mercury fluxes from the forest floor of the Adirondacks. *Environ. Pollut.* **2009**, *157*, 592−600.
(56) Zheng, W.; Obrist, D.; Weis, D.; Bergquist, B. A. Mercury isotope compositions across North American forests. *Global Biogeochem. Cycles* **2016**, *30*, 1475−1492.
(57) Jiskra, M.; Wiederhold, J. G.; Skyllberg, U.; Kronberg, R.-M.; Hajdas, I.; Kretzschmar, R. Mercury Deposition and Re-emission Pathways in Boreal Forest Soils Investigated with Hg Isotope Signatures. *Environ. Sci. Technol.* **2015**, *49*, 7188−7196.
(58) Wang, X.; Lin, C.-J.; Feng, X.; Yuan, W.; Fu, X.; Zhang, H.; Wu, Q.; Wang, S. Assessment of Regional Mercury Deposition and Emission Outflow in Mainland China. *J. Geophys. Res.: Atmos.* **2018**, *123*, 9868−9890.
(59) Chen, H. S.; Wang, Z. F.; Li, J.; Tang, X.; Ge, B. Z.; Wu, X. L.; Wild, O.; Carmichael, G. R. GNAQPMS-Hg v1.0, a global nested atmospheric mercury transport model: model description, evaluation and application to trans-boundary transport of Chinese anthropogenic emissions. *Geosci. Model Dev.* **2015**, *8*, 2857−2876.
(60) Ci, Z. J.; Zhang, X. S.; Wang, Z. W.; Niu, Z. C.; Diao, X. Y.; Wang, S. W. Distribution and air-sea exchange of mercury (Hg) in the Yellow Sea. *Atmos. Chem. Phys.* **2011**, *11*, 2881−2892.

DOI: 10.1021/acs.est.9b05016
Environ. Sci. Technol. 2019, 53, 13748−13756